BJR

https://doi.org/10.1259/bjr.20170872

Received: 16 November 2017 | Revised: 10 October 2018 | Accepted: 12 October 2018

Cite this article as:
Novak J, Withey SB, Lateef S, MacPherson L, Pinkey B, Peet AC. A comparison of pseudo-continuous arterial spin labelling and dynamic susceptibility contrast MRI with and without contrast agent leakage correction in paediatric brain tumours. *Br J Radiol* 2019; **91**: 20170872.

FULL PAPER

A comparison of pseudo-continuous arterial spin labelling and dynamic susceptibility contrast MRI with and without contrast agent leakage correction in paediatric brain tumours

[1,2]JAN NOVAK, PhD, [1,2,3]STEPHANIE BARBARA WITHEY, PhD, [1]SHAHEEN LATEEF, PgCert, [1]LESLEY MACPHERSON, MBChB, FRCR, [1]BENJAMIN PINKEY, MBChB, FRCR and [1,2]ANDREW C PEET, PhD FRCPCH

[1]Birmingham Children's Hospital, Birmingham, UK
[2]Cancer Sciences, University of Birmingham, Birmingham, UK
[3]RRPPS, University Hospitals Birmingham NHS Foundation Trust, Birmingham, UK

Address correspondence to: Professor Andrew C Peet
E-mail: *a.peet@bham.ac.uk*

Jan Novak and Stephanie Barbara Withey have contributed equally to this study and should be considered as co-first authors.

Objective: To investigate correlations between MRI perfusion metrics measured by dynamic susceptibility contrast and arterial spin labelling in paediatric brain tumours.

Methods: 15 paediatric patients with brain tumours were scanned prospectively using pseudo-continuous arterial spin labelling (ASL) and dynamic susceptibility contrast (DSC-) MRI with a pre-bolus to minimise contrast agent leakage. Cerebral blood flow (CBF) maps were produced using ASL. Cerebral blood volume (CBV) maps with and without contrast agent leakage correction using the Boxerman technique and the leakage parameter, K_2, were produced from the DSC data. Correlations between the metrics produced were investigated.

Results: Histology resulted in the following diagnoses: pilocytic astrocytoma (n = 7), glioblastoma (n = 1), medulloblastoma (n = 1), rosette-forming glioneuronal tumour of fourth ventricle (n = 1), atypical choroid plexus papilloma (n = 1) and pilomyxoid astrocytoma (n = 1). Three patients had a non-invasive diagnosis of low-grade glioma. DSC CBV maps of T_1-enhancing tumours were difficult to interpret without the leakage correction. CBV values obtained with and without leakage correction were significantly different (p < 0.01). A significant positive correlation was observed between ASL CBF and DSC CBV (r = 0.516, p = 0.049) which became stronger when leakage correction was applied (r = 0.728, p = 0.002). K_2 values were variable across the group (mean = 0.35, range = −0.49 to 0.64).

Conclusion: CBV values from DSC obtained with and without leakage correction were significantly different. Large increases in CBV were observed following leakage correction in highly T_1-enhancing tumours. DSC and ASL perfusion metrics were found to correlate significantly in a range of paediatric brain tumours. A stronger relationship between DSC and ASL was seen when leakage correction was applied to the DSC data. Leakage correction should be applied when analysing DSC data in enhancing paediatric brain tumours.

Advances in knowledge: We have shown that leakage correction should be applied when investigating enhancing paediatric brain tumours using DSC-MRI. A stronger correlation was found between CBF derived from ASL and CBV derived from DSC when a leakage correction was employed.

INTRODUCTION

Brain tumours are the biggest cause of death from cancer in children.[1] Radiological assessment is one of the key tools used in the management of this patient cohort. The primary imaging modality now employed is MRI which provides a clear picture of the internal soft tissue structure of the brain. Advanced MRI techniques are able to probe metabolism, blood flow and cellularity via a range of methods.[2] Perfusion MRI, which provides estimates of cerebral blood flow (CBF) and relative cerebral blood volume (rCBV), has become increasingly pertinent as the use of antivascular and anti-angiogenic

treatments are becoming more commonplace[3] and has demonstrated relationships with tumour grade[4,5] and long-term survival.[6]

Two widely-used methods for measuring perfusion in the brain are dynamic susceptibility contrast (DSC-) MRI and arterial spin labelling (ASL). DSC-MRI involves the injection of a contrast agent followed by rapid tracking of the bolus via MR imaging.[7] The use of DSC-MRI has been reported in paediatrics[5,8] but a number of issues have prevented it from being implemented routinely, such as the requirement of a cannula and pressure injector, increasing concerns over the use of gadolinium contrast agents[9] and the need for an arterial input function for fully quantitative analysis.[10] DSC data analysis methods[11] assume that the injected contrast agent remains intravascular so that the effects of contrast agent on T_1 can be ignored. rCBV can therefore be calculated as the area underneath the change in effective transverse relaxation time, ΔR_2^*, graph. This is not the case in many brain tumours due to blood brain barrier breakdown.[12] Leakage of contrast agent into the extravascular extracellular space (EES) during the DSC scan affects the signals produced in two competing ways. Contrast agent shortens T_1 values of tissue water within the EES, resulting in an increase in MR signal during the DSC scan which competes with the MR signal arising due to intravascular contrast agent and resulting in an underestimation of rCBV. Conversely, T_2/T_2^* effects arise due to changes in susceptibility differences between the EES and intravascular compartments reducing the MR signal so that it does not recover to baseline during the DSC scan. This results in overestimation of rCBV. Where contrast agent extravasation is particularly rapid rCBV can be calculated as negative as the signal increase due to T_1 effects is greater than the signal reduction due to T_2^* effects. Leakage effects can be addressed by giving a loading dose of contrast agent prior to the DSC acquisition,[13,14] careful choice of sequence parameters to minimise the effect of leakage on the signal-time course[14,15] and by using post-processing methods to correct for contrast agent leakage.[16–20] The Boxerman technique[16,19] uses the signal-time course obtained from a whole-brain mask of non-enhancing pixels to correct the leakage-affected DSC signal-time course, resulting in a corrected cerebral blood volume (CBV). A parameter representing the amount of leakage that has taken place, K_2, is also obtained.

ASL does not require an injection of contrast agent, instead using a labelling slice placed in the neck to label blood flowing into the imaging volume.[21] ASL has yet to establish itself into routine clinical practice due to its inherently low signal-to-noise-ratio (SNR), limited spatial resolution, a lack of harmonisation between the protocols available on different scanners and limited clinical evidence of usefulness. Modern hardware improvements including the increased availability of 3T scanners and pulse sequence development including pseudo-continuous ASL (pCASL),[22] Look-Locker[23] and combined gradient and spin echo[24] readouts have, in part, addressed SNR and scan length limitations. The recent publication of a consensus paper on recommended clinical protocols has provided a solid foundation for ASL to be implemented clinically in both adults and children.[21] The recommendations clearly point to the use of pCASL, preferably with a three-dimensional readout. This is due to the high SNR afforded by the labelling scheme/readout combination and also the near-complete head coverage that can be achieved in a clinically-acceptable timescale.[21]

The lack of requirement for contrast agent administration in ASL imaging is an obvious advantage over DSC-MRI in the imaging of paediatric brain tumours. It is important, however, to assess the relationship between techniques which provide measures of similar metrics. A previous study investigating paediatric brain tumours using ASL and DSC found significant correlations between metrics in grey matter but found no significant correlation in tumours;[25] however, leakage correction was not applied to the DSC data. A subsequent study has shown large differences in the extent of leakage correction between high- and low-grade paediatric brain tumours suggesting that leakage correction is important when analysing DSC data in paediatric brain tumours.[26] Finally, Dallery et al[27] showed differences in leakage correction parameters between high- and low-grade paediatric brain tumours, although differences between corrected CBV values were not presented.

In this study we compare CBV measured by DSC and CBF measured by ASL in paediatric brain tumour patients. We apply the Boxerman method of leakage correction[19] and compare corrected and uncorrected DSC CBV maps to the ASL data to assess the importance of this post-processing step.

METHODS AND MATERIALS

This prospective study was approved by the East Midlands-Derby Research Ethics Committee (REC 04/MRE04/41), operating under the rules of Declaration of Helsinki 1975 (and as revised in 1983). Informed parental consent was obtained from all subjects. A total of 15 paediatric patients with a diagnosis of a brain tumour by the local Neuro-Oncology Multidisciplinary Team underwent additional ASL and DSC scans as part of an MRI performed for routine clinical assessment.

Patients

Patients were eligible for inclusion if they had a cannula *in situ* for administration of contrast agent via a power injector – this included those undergoing general anaesthetic (mostly those under 6 years of age and approximately 50% of our paediatric brain tumour cohort) or for clinical necessity (an additional 10%)–residual tumour greater than 1 cm^3 in volume, patients with tumours which were not located close to the brain stem and those without metal implants so that susceptibility artefacts would not render data unanalysable. These patients were scanned on an advanced imaging list (of which there are approximately three examinations per month) to allow for the additional time needed for research scans. Since the primary aim of the study was to compare DSC and ASL rather than to determine perfusion characteristics of the tumours, patients were eligible irrespective of the treatment which they had received up to the point of the MRI. All data was acquired on a Philips Achieva 3T TX system (Best, The Netherlands) using a 32-channel head coil.

Imaging protocol

Arterial spin labelling MRI

A pseudo-continuous ASL (pCASL) sequence was used. Six transverse slices with a thickness of 7 mm and a matrix size of 64 × 64 pixels and one post-labelling delay at 1400 ms were acquired using a flip angle of 40° and a single shot EPI readout with 30 averages. The voxel volume was 3.75 × 3.75 × 7 mm. The pCASL labelling slab was placed 20 mm below the imaging slices and had duration 1400 ms. Vascular crushing and background suppression were not used for this study as there is no established method for optimisation for these in both brain tumours and the paediatric population. M0 maps were acquired using the same parameters as the ASL images minus the pCASL labelling and with the repetition time (TR) increased to 10 s using a single average.

Dynamic susceptibility contrast MRI

Prior to the DSC scan a high-resolution T_2 weighted turbo spin echo scan with the same coverage was acquired for the purpose of defining regions-of-interest (ROI) [TR/echo time (TE) = 4000/100 ms, matrix = 144 × 144]. The DSC-MRI scan was a transverse field-echo echo planar imaging scan (TR/TE = 1865/40 ms, field-of-view (FOV) =240 × 240 mm, matrix = 96 × 96, voxel volume = 2.5 × 2.5 x 3.5 mm) with flip angle of 20°. 30 slices with a slice thickness of 3.5 mm each were acquired to cover the whole brain. The temporal resolution of the DSC scan was 1.86 s which was repeated 60 times. Contrast agent (Dotarem, Guerbet, France) was administered via a power injector through a cannula inserted into a suitable vein. The total dose of contrast agent given was 0.1 mmol/kg in two stages – the first half-dose as a pre-bolus prior to the high-resolution T_2 weighted acquisition to allow minimisation of T_1 effects and the second half-dose at the start of time point six in the DSC data acquisition, with each injection followed by a volume of up to 10 mls of saline. The injection rate used was 3 ml s^{-1}.

Pre- and post-contrast MRI

Pre- and post-contrast T_1 weighted TSE scans were acquired with the following parameters (TR = 600–825 ms, TE = 10 ms, flip angle = 50–70°, field-of-view = 230 × 230 mm, matrix = 512 × 512, voxel volume = 0.45 × 0.45 x 5 mm, number of slices = 30–36).

Data analysis

Both DSC and ASL data analyses were performed using software developed in-house written in the Python programming language (v2.7, Python Software Foundation, http://www.python.org).

Arterial Spin Labelling MRI

CBF maps were produced from the ASL images using the method suggested in the recent consensus paper.[21] The ASL images acquired with labelling were subtracted from the control images – those acquired without labelling pulse - to produce a perfusion-weighted image. Quantification was achieved by using equation 1.

$$\mathrm{CBF} = \frac{6000\cdot\lambda\cdot(\mathrm{SI_{control}}-\mathrm{SI_{label}})\cdot e^{\frac{\mathrm{PLD}}{\mathrm{T_{1(blood)}}}}}{2\cdot\alpha\cdot \mathrm{T_{1(blood)}}\cdot \mathrm{SI_{PD}}\cdot(1-e)^{-\frac{\tau}{\mathrm{T_{1(blood)}}}}}\ [\mathrm{ml/100\ g/min}] \quad [1]$$

where λ is the blood-brain barrier partition coefficient (assumed to be 0.9 ml g^{-1}), $SI_{control}$ is the signal intensity of the control image, SI_{label} is the signal intensity of the label image, T_1 (blood) is the T_1 value of arterial blood (assumed to be 1.650 s at 3T), TI_1 is the post-labelling delay and α is the labelling efficiency assumed to be 0.85. All assumed values were taken from Alsop et al.[21]

Dynamic susceptibility contrast MRI

Signal-time curves were obtained from the DSC time course on a pixel-by-pixel basis and converted to the change in T_2* relaxation time, ΔR_2*, using:

$$\Delta \mathrm{R_2}*\,(\mathrm{t}) = -\frac{1}{\mathrm{TE}}\ln\left(\frac{\mathrm{S\,(t)}}{\mathrm{S\,(0)}}\right) \quad [2]$$

where S(t) and S(0) are the signal intensities at time, *t*, and baseline respectively and TE is the time-to-echo of the DSC sequence. The baseline signal intensity was calculated by averaging the signal from the first six time points. Pixel-by-pixel uncorrected rCBV values were calculated by integrating over the R_2*-time curves. Corrected rCBV values were calculated using the method outlined in.[16,19] In brief, this model takes into account both the T_1 and T_2 effects from contrast agent extravasation and aims to correct for them. Corrected rCBV ($rCBV_{corr}$) is calculated by integrating over the corrected R_2*-time curves, $R_{2,corr}$*(t):

$$\Delta \mathrm{R_{2,corr}}*\,(\mathrm{t}) = \Delta\widetilde{\mathrm{R}}_2^{*}\,(\mathrm{t}) + \mathrm{K_2}\int_0^{\mathrm{t}}\Delta\overline{\mathrm{R}}_2^{*}\left(\mathrm{t}'\right)\mathrm{dt}' \quad [3]$$

where $\Delta\widetilde{R}_2^{*}(t)$ is the uncorrected ΔR_2*, $\Delta\overline{R}_2^{*}(t')$ is the ΔR_2* obtained over the whole brain and therefore provides an estimate of the ΔR_2* without allowing for leakage and K_2 is a term reflecting the effects of leakage on both T_1 and T_2* and is estimated by fitting the uncorrected ΔR_2* to the following equation:

$$\Delta\widetilde{\mathrm{R}}_2\,(\mathrm{t}) \equiv \mathrm{K_1}\cdot\Delta\overline{\mathrm{R}}_2^{*}\,(\mathrm{t}) - \mathrm{K_2}\int_0^{\mathrm{t}}\Delta\overline{\mathrm{R}}_2^{*}\left(\mathrm{t}'\right)\mathrm{dt}' \quad [4]$$

A positive K_2 indicates that T_1 effects dominate the resulting signal-time curve while a negative K_2 indicates T_2*-dominant effect.[19] K_1 is purely a constant of proportionality. K_1 and K_2 were both obtained by least-squares fitting of the uncorrected ΔR_2* to equation 4 using the whole-brain average $\Delta\overline{R}_2^{*}(t)$ as obtained from non-enhancing pixels in the brain and excluding signal from the ventricles.

Pre- and post-contrast MRI

The pre- and post-contrast T_1 weighted images were registered to one another using the MERIT module in MeVisLab (v2.8.2, MeVis Medical Solutions AG, Germany) and then reformatted to cover the same volume as the high-resolution T_2 weighted images. An image of the level of contrast enhancement was computed using:

$$\text{Contrast enhancement} = \frac{\mathrm{Signal_{post-contrast}} - \mathrm{Signal_{pre-contrast}}}{\mathrm{Signal_{pre-contrast}}}\times 100 \quad [5]$$

Table 1. Patient cohort demographics

Sex	Age (years)	Tumour location	Histology/diagnosis	NF1[a]	Surgery	Chemotherapy
M	11.3	Thalamus	Pilocytic astrocytoma	Y	Y	First: vincristine, carboplatin Second: vinblastine Third: vincristine actinomycin
M	8.8	Cerebellum	Rosette-forming glioneuronal tumour of fourth ventricle	N	Y	First: vincristine, carboplatin, etoposide Second: erlotinib
F	4.8	Optic chiasm	Pilocytic astrocytoma	N	Y	First: vincristine, carboplatin Second vinblastine
M	3.9	Optic chiasm	Pilocytic astrocytoma	N	Y	First vincristine, carboplatin, etoposide Second vincristine actinomycin
M	2.8	Optic chiasm	Pilocytic astrocytoma	N	N	First: vincristine, carboplatin Second: vincristine, actinomycin
F	5.6	Optic pathway	Pilocytic astrocytoma	Y	N	First: vincristine, carboplatin Second: vincristine, actinomycin
F	1.6	Right parietal	Atypical choroid plexus papilloma	N	Y	Cyclophosphamide, etoposide, carboplatin, vincristine
M	2.1	Left hemispheric	Glioblastoma	N	Y	First: carboplatin, etoposide, methotrexate, vincrisine, cyclophosphamide Second bevacizumab, temozolomide
M	9.8	Cerebellum	Medulloblastoma	N	N	None
F	5.3	Optic pathway	Low-grade glioma	Y	N	First: vincristine, carboplatin Second vincristine, cyclophosphamide
M	1.7	Hypothalamus	Pilocytic astrocytoma	N	Y	Vincristine, carboplatin
M	1.6	Optic chiasm	Pilocytic astrocytoma	N	Y	Vincristine, carboplatin
F	3.7	Pons	Low-grade glioma	N	N	Vincristine, carboplatin
M	2.9	Optic chiasm	Pilomyxoid astrocytoma	N	Y	First: vincristine, carboplatin Second vinblastine
F	5.3	Cerebellar peduncle	Low-grade glioma	Y	N	None

[a]NF1 = neurofibromatosis Type 1.

Regions of interest

ROI were drawn around the whole tumour by JN, a scientist with 6 years' research experience in paediatric brain tumours, on the high-resolution T_2 weighted images using clinically-acquired MRI scans for reference. Large areas of cyst were excluded. All ROIs were checked and amended where necessary by a consultant radiologist who is a member of the Neuro-Oncology Multidisciplinary Team with 2 years of experience (BP). The ROIs were transferred to the perfusion maps and to the contrast enhancement images calculated using equation 5. Mean whole-tumour CBF, uncorrected and corrected CBV, K_2 and contrast enhancement were calculated. Tumour size was calculated from the registered images by multiplying the number of voxels in the tumour ROI by the voxel volume. Further statistical analysis using SPSS (IBM v.24) was performed.

RESULTS

Table 1 summarises the demographics, diagnosis along with neurofibromatosis Type 1 (NF1) status and any tumour treatment prior to the DSC-ASL investigation for the 15 patients included in the study. The cohort comprised six female patients and nine male patients. The age range for the group was 1.6 to 11.3 years. Low-grade gliomas included pilocytic astrocytoma (n = 7), a rosette-forming glio-neuronal tumour of the fourth ventricle (n = 1), atypical choroid plexus papilloma (n = 1) and pilomyxoid astrocytoma (n = 1). High-grade gliomas included glioblastoma (n = 1) and medulloblastoma (n = 1). A diagnosis of low-grade glioma was made by the Neuro-Oncology Multidisciplinary Team on clinical and imaging grounds without a biopsy on three patients.

Table 2 shows mean ASL CBF and DSC CBV values – with and without leakage correction – and the percentage contrast agent enhancement as calculated from the pre- and post-contrast T_1 weighted images. Percentage contrast agent enhancement is not shown for two of the 15 patients as one or more of the pre- or post-contrast images were not available for analysis. Mean K_2 was positive in eight tumours indicating T_1-dominant leakage; K_2 was negative in four tumours indicating T_2*-dominant leakage and negligible in three tumours suggesting leakage was not an issue. In particular, two tumours with high levels of contrast enhancement had negative uncorrected CBV. On correction, both were found to have T_1-dominant leakage with leakage correction resulting in a large increase in CBV and the highest positive K_2 values of the cohort (tumour 1: CBV: −0.22 ml 100 g^{-1} to 2.13 ml 100 g^{-1}, K_2 = 0.64; tumour 2:

Table 2. Mean whole-tumour parameters. Presented are the mean values of CBF calculated from the ASL images, CBV values - both uncorrected and with leakage correction–and K_2 from DSC imaging. The percentage amount of contrast enhancement as calculated from the pre- and post-contrast T_1 images for 13 patients is shown (at least one of the pre- and post-contrast images were not available for two of the patients in the study)

Diagnosis	Tumour volume cm^3	CBF ml 100 g^{-1} min^{-1}	CBV uncorrected ml 100 g^{-1}	CBV corrected ml 100 g^{-1}	K_2	Amount of contrast enhancement
Pilocytic astrocytoma	5.58	79.49	4.08	4.34	−0.49	107.0%
Rosette-forming glioneuronal tumour of fourth ventricle	22.38	63.91	1.79	3.30	0.36	–
Pilocytic astrocytoma	4.70	86.12	2.21	2.71	0.08	84.6%
Pilocytic astrocytoma	40.64	56.03	−0.22	2.13	0.64	109.7%
Pilocytic astrocytoma	28.02	52.50	1.33	2.77	0.41	52.2%
Pilocytic astrocytoma	4.70	48.21	1.26	1.85	0.16	5.2%
Atypical choroid plexus papilloma	1.40	10.94	2.33	2.49	−0.42	22.5%
Glioblastoma	33.45	10.24	1.76	1.89	−0.60	35.6%
Medulloblastoma	33.25	38.69	1.56	1.96	0.17	-
Low-grade glioma	3.19	82.62	3.81	4.06	0.26	23.1%
Pilocytic astrocytoma	24.87	21.57	1.02	1.29	0.05	12.7%
Pilocytic astrocytoma	30.32	23.54	1.29	1.96	0.12	128.1%
Low-grade glioma	10.68	74.63	2.41	2.68	0.04	10.2%
Pilomyxoid astrocytoma	1.12	20.22	−0.30	1.24	0.57	170.0%
Low-grade glioma	45.94	54.15	3.32	3.54	−0.36	7.8%

ASL, arterial spin labelling; CBF, cerebral blood flow; CBV, cerebral blood volume; DSC, dynamic susceptibility contrast;

CBV = −0.30 ml 100 g^{-1} to 1.24 ml 100 g^{-1}, K_2 = 0.57). Two other tumours with high levels of contrast enhancement and low uncorrected CBV had similar results to a lesser degree. Tumours with low levels of enhancement and/or high uncorrected CBV had K_2 values closer to zero (both positive and negative). Median K_2 for the five most enhancing tumours was 0.12 (range = 0.08 to 0.64) compared to 0.08 (range = −0.49 to 0.64) across the entire cohort. The median increase in CBV after leakage correction in this group was 52% as opposed to 23% in the remaining tumours.

The low-grade tumour in Figure 1 shows a high level of contrast agent uptake within the tumour which has caused CBV within the lesion to be underestimated when leakage correction is not applied, resulting in a void within the tumour on the uncorrected CBV map. When corrected heterogeneous CBV values are seen within the tumour, CBV values outside of the tumour are largely unaffected by the correction. High K_2 values in the tumour compared to surrounding tissue reflect the amount of leakage correction required. Mean K_2 was high at 0.64 demonstrating

Figure 1. Axial images from a 3-year-old male with a pilocytic astrocytoma. The patient had previously undergone surgery as well as first- and second-line chemotherapy. Shown from left to right are: post-contrast T_1 weighted image showing vivid contrast enhancement in the tumour, uncorrected and corrected CBV maps produced from the DSC data and the K_2 map for the same slice. Mean uncorrected and corrected tumour CBV were −0.22 ml 100 g^{-1} and 2.13 ml 100 g^{-1} respectively; mean K_2 was 0.64 and mean contrast enhancement was 109.7%. CBV, cerebral blood volume; DSC, dynamic susceptibility contrast.

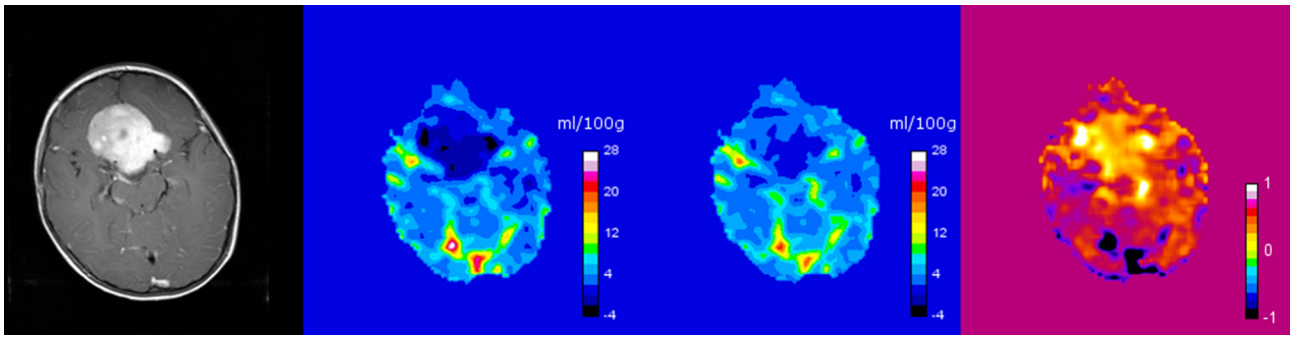

Figure 2. Axial images from a 4-year-old female with a pilocytic astrocytoma treated with first- and second-line chemotherapy prior to MRI. Top-left: T_2 weighted image, top-right: T_1 weighted post-contrast image showing vivid contrast enhancement within the solid part of the tumour, bottom-left: CBF map derived from the ASL images and, bottom-right: leakage-corrected CBV map derived from the DSC images. ASL CBF was 86.12 ml 100 g^{-1} min^{-1}; DSC leakage-corrected CBV was 2.71 ml 100 g. ASL, arterial spin labelling; CBF, cerebral blood flow; CBV, cerebral blood volume; DSC, dynamic susceptibility contrast.

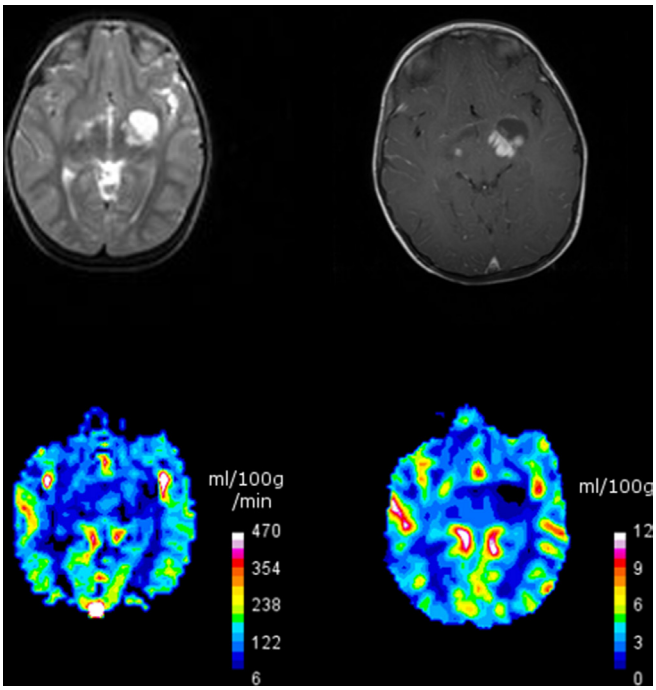

Figure 3. Plots showing the correlation between mean DSC CBV and ASL CBF values in tumour ROI. The top plot shows mean values taken from CBV maps without leakage correction (r = 0.516, p = 0.049). The bottom plot shows mean values taken from CBV maps with T_1 and T_2 correction (r = 0.728, p = 0.002). ASL, arterial spin labelling; CBF, cerebral blood flow; CBV, cerebral blood volume; DSC, dynamic susceptibility contrast; ROI, regions of interest.

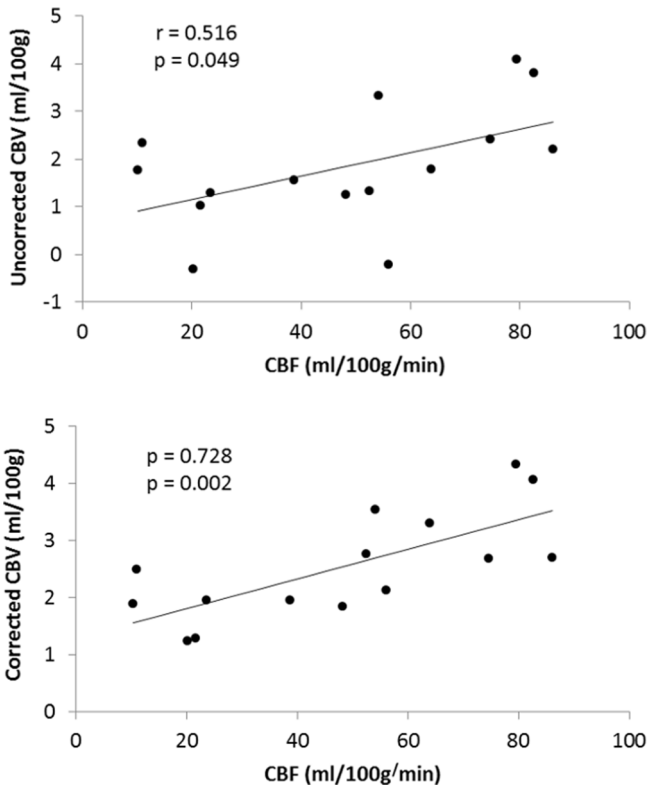

the necessity for leakage correction. Good agreement is observed between CBF maps produced from ASL and leakage-corrected CBV maps (Figure 2).

A significant correlation was found between tumour CBF and patient age (r = 0.559, p = 0.030). No correlation was observed between age and uncorrected CBV (r = 0.434, p = 0.106) but was observed for the corrected (r = 0.560, p = 0.030) CBV data. Tumour volume was not found to correlate significantly with any other parameter. Median tumour volume was 22.4 cm^3 (range = 1.1–45.9 cm^3). CBV values without the correction were consistently lower than those which had undergone the Boxerman correction for leakage (median = 1.76 ml 100 g^{-1} *vs* 2.49 ml 100 g^{-1} respectively). A paired t-test showed a significant difference between the corrected and non-corrected CBV values from the tumour ROI ($p < 0.001$). K_2 values were variable (median = 0.16, range = −0.49–0.64) as were levels of contrast agent enhancement (median = 35.6%, range = 5.2–170.0%) although the two parameters did not correlate significantly (r = 0.411, p = 0.163).

Mean tumour CBF calculated from the ASL images were tested against the mean tumour CBV values calculated from the DSC images to investigate correlations between the two methods as shown in Figure 3. A significant positive correlation was found between CBF and the uncorrected CBV (r = 0.516, p = 0.049) and a stronger correlation was found between CBF and corrected CBV (r = 0.728, p = 0.002).

DISCUSSION

We have shown a significant correlation between CBV measured by DSC and CBF measured by ASL in children's brain tumours. This correlation was improved when leakage correction was applied to the DSC data. When the blood brain barrier has been breached, contrast agent leaks from blood vessels resulting in T_1 and T_2* changes in the extracellular extravascular space. We employed both a pre-load of contrast agent and post-processing techniques to correct for these effects.[16] The results suggest that ASL could be an alternative perfusion technique in paediatric patients where DSC data acquisition is difficult.

Across the patient cohort a significant difference in mean tumour CBV values with and without leakage correction was observed. Some tumours required more correction than others, reflected in the large range of K_2 values shown in Table 2. We employed the Boxerman technique[16] to correct DSC data but included the amendment present in[19] where K_2 was allowed to be either positive or negative. A positive K_2 is associated with T_1-dominant

contrast agent leakage while a negative K_2 is associated with T_2*-dominant leakage. Tumours in our group were found to have a mixture of these effects.

Low-grade tumours, such as pilocytic astrocytomas, demonstrating high enhancement on post-contrast T_1 weighted images were often observed to have artificially low (sometimes negative or zero) uncorrected CBV values (Table 2), making clinical interpretation challenging. Following leakage correction in these tumours a large increase in CBV is observed and a large positive K_2, indicating T_1-dominant leakage[19,28] was present requiring significant correction. This is illustrated in Figure 1 which shows an uncorrected and corrected CBV map. Once corrected and rescaled, more detail showing the heterogeneity and range of CBV values within the tumour is observed, K_2 is large and positive and CBV has increased throughout the tumour.

Leakage effects have previously been investigated qualitatively for the grading of paediatric brain tumours, with the type of leakage as reflected by signal-intensity time curve shape–T_1-dominant or T_2*-dominant and return to baseline–being associated with low- and high-grade tumours respectively.[28] This suggests that additional information is available from DSC-MRI data when leakage correction is applied.

Good agreement was observed between ASL CBF and DSC CBV maps. Although qualitative assessment is important from a radiological perspective it is important to develop quantitative imaging biomarkers that are robust.[29] A recent paediatric brain tumour study showed no significant correlation between ASL and DSC metrics between tumours;[25] however, correlations were shown for controls only, suggesting a problem only observed in tumour regions. No leakage correction was applied and the comparison in the tumours was made using CBF measured by both ASL and DSC. Questions still remain over the reliability of CBF measurements from DSC[30] due to variations in how it is calculated, and CBV is still the most common DSC parameter presented in the literature. A recent study[31] found a significant correlation between pre-treatment ASL CBF and DSC CBV in paediatric astrocytic tumours. Leakage correction was employed; however, the results of this were not reported.

The Boxerman technique, while fairly simple to implement, relies on having normal brain tissue within the imaging volume in order to correct leakage-affected contrast agent concentration-time curves. This may not always be possible especially with large brain tumours or where there is substantial oedema present. Other correction techniques have been presented in the literature.[16,17,19] We also administered a pre-bolus of half the full contrast agent dose to all patients prior to the DSC measurements to reduce T_1 effects from contrast agent extravasation. Leakage effects resulting in difficult-to-interpret CBV maps were still observed, particularly in highly-enhancing tumours such as pilocytic astrocytomas, suggesting that the use of a pre-bolus is limited in this patient group. Currently there is no consensus on the optimal dose or timing of the pre-bolus administration although a recent study suggested that a second full dose was optimal.[13] There is insufficient safety information to recommend this approach at present, particularly in children, and so we follow an internationally-accepted protocol for DSC-MRI in paediatric patients in Europe (International Society for Paediatric Oncology Europe, SIOPE).

Our patient cohort was relatively small due to the challenges of performing multiple advanced imaging techniques on children. Insertion of venous cannulas in young children is difficult and central venous lines are not considered compatible with power injectors. Our patient cohort is relatively young, as younger patients are more likely to be scanned under general anaesthetic with a cannula in place. ASL measurements may have been improved by the normalisation of signal to unaffected tissue such as grey or white matter; however, this was difficult in some patients due to the large tumour sizes in them resulting in little healthy tissue within the ASL FOV. The subtraction analysis to assess levels of contrast agent enhancement was performed retrospectively with data acquired as part of clinical practice. For this reason, the timings between pre- and post-contrast T_1 acquisitions were not controlled and therefore variable between patients. This may explain why the level of enhancement did not always reflect the K_2 value for a particular patient. Finally, the tumour group included in this study along with the treatments undergone prior to imaging is heterogeneous therefore the level of vessel leakage may not mirror that of a different cohort. However, many of the adjuvant treatments used in paediatric tumours, particularly chemotherapy for low-grade gliomas, have an antivascular effect and so we would expect vessel leakage correction to be even more important in untreated tumours. The results of this study show that no matter at what point in treatment, if a tumour is enhancing, leakage correction is necessary to produce more accurate CBV values.

CONCLUSIONS

In this study we have demonstrated the importance of leakage correction for DSC imaging of enhancing paediatric brain tumours and its use in both qualitative and quantitative assessment. We found that CBF measured by ASL correlated well with CBV measured by DSC-MRI in paediatric brain tumours with the correlation improving once leakage correction had been applied. The amount of leakage correction required was highest in tumours showing high post-contrast T_1 weighted enhancement combined with low CBV. These tumours showed T_1-dominant leakage effects and large increases in CBV were observed following correction. We have also shown data that suggests a pre-bolus of contrast agent delivered prior to a DSC scan is not sufficient to reduce leakage effects alone, especially in highly-enhancing tumours. ASL is proving to be an alternative method for measuring perfusion in paediatric patients where DSC-MRI can prove challenging.

ACKNOWLEDGMENT

This study was funded by a Birmingham Women's and Children's Hospital Research Foundation project grant. We also acknowledge funding from the CRUK and EPSRC Cancer Imaging Programme at the Children's Cancer and Leukaemia Group (CCLG) in association with the MRC and Department of Health (England) (C7809/A10342) and Help Harry Help Others

Charity. Professor Peet is funded through an NIHR Research Professorship, 13-0053. We would like to acknowledge the MR radiographers at Birmingham Children's Hospital for scanning the patients in this study.

REFERENCES

1. UKCR, Children's cancers mortality by cancer type 2017.
2. Peet AC, Arvanitis TN, Leach MO, Waldman AD. Functional imaging in adult and paediatric brain tumours. *Nat Rev Clin Oncol* 2012; **9**: 700–11. doi: https://doi.org/10.1038/nrclinonc.2012.187
3. Farid N, Almeida-Freitas DB, White NS, McDonald CR, Kuperman JM, Almutairi AA, et al. Combining diffusion and perfusion differentiates tumor from bevacizumab-related imaging abnormality (bria). *J Neurooncol* 2014; **120**: 539–46. doi: https://doi.org/10.1007/s11060-014-1583-2
4. Yeom KW, Mitchell LA, Lober RM, Barnes PD, Vogel H, Fisher PG, et al. Arterial spin-labeled perfusion of pediatric brain tumors. *AJNR Am J Neuroradiol* 2014; **35**: 395-401. doi: https://doi.org/10.3174/ajnr.A3670
5. Ho CY, Cardinal JS, Kamer AP, Kralik SF. Relative cerebral blood volume from dynamic susceptibility contrast perfusion in the grading of pediatric primary brain tumors. *Neuroradiology* 2015; **57**: 299–306. doi: https://doi.org/10.1007/s00234-014-1478-0
6. Hipp SJ, Steffen-Smith E, Hammoud D, Shih JH, Bent R, Warren KE. Predicting outcome of children with diffuse intrinsic pontine gliomas using multiparametric imaging. *Neuro Oncol* 2011; **13**: 904–9. doi: https://doi.org/10.1093/neuonc/nor076
7. Calamante F. Arterial input function in perfusion MRI: a comprehensive review. *Prog Nucl Magn Reson Spectrosc* 2013; **74**: 1–32. doi: https://doi.org/10.1016/j.pnmrs.2013.04.002
8. Lam S, Lin Y, Warnke PC. Permeability imaging in pediatric brain tumors. *Transl Pediatr* 2014; **3**: 218–28. doi: https://doi.org/10.3978/j.issn.2224-4336.2014.07.01
9. Ramalho M, Ramalho J, Burke LM, Semelka RC. Gadolinium retention and toxicity-an update. *Adv Chronic Kidney Dis* 2017; **24**: 138–46. doi: https://doi.org/10.1053/j.ackd.2017.03.004
10. Withey SB, Novak J, MacPherson L, Peet AC. Arterial input function and gray matter cerebral blood volume measurements in children. *J Magn Reson Imaging* 2016; **43**: 981–9. doi: https://doi.org/10.1002/jmri.25060
11. Østergaard L. Principles of cerebral perfusion imaging by bolus tracking. *J Magn Reson Imaging* 2005; **22**: 710–7. doi: https://doi.org/10.1002/jmri.20460
12. Essig M, Anzalone N, Combs SE, Dörfler À, Lee SK, Picozzi P, et al. MR imaging of neoplastic central nervous system lesions: review and recommendations for current practice. *AJNR Am J Neuroradiol* 2012; **33**: 803–17. doi: https://doi.org/10.3174/ajnr.A2640
13. Boxerman JL, Prah DE, Paulson ES, Machan JT, Bedekar D, Schmainda KM. The Role of preload and leakage correction in gadolinium-based cerebral blood volume estimation determined by comparison with MION as a criterion standard. *AJNR Am J Neuroradiol* 2012; **33**: 1081–7. doi: https://doi.org/10.3174/ajnr.A2934
14. Leu K, Boxerman JL, Ellingson BM. Effects of MRI protocol parameters, preload injection dose, fractionation strategies, and leakage correction algorithms on the fidelity of dynamic-susceptibility contrast MRI estimates of relative cerebral blood volume in gliomas. *AJNR Am J Neuroradiol* 2017; **38**: 478–84. doi: https://doi.org/10.3174/ajnr.A5027
15. Boxerman JL, Paulson ES, Prah MA, Schmainda KM. The effect of pulse sequence parameters and contrast agent dose on percentage signal recovery in DSC-MRI: implications for clinical applications. *AJNR Am J Neuroradiol* 2013; **34**: 1364–9. doi: https://doi.org/10.3174/ajnr.A3477
16. Boxerman JL, Schmainda KM, Weisskoff RM. Relative cerebral blood volume maps corrected for contrast agent extravasation significantly correlate with glioma tumor grade, whereas uncorrected maps do not. *AJNR Am J Neuroradiol* 2006; **27**: 859–67.
17. Leigh R, Jen SS, Varma DD, Hillis AE, Barker PB. Arrival time correction for dynamic susceptibility contrast MR permeability imaging in stroke patients. *PLoS One* 2012; **7**: e52656. doi: https://doi.org/10.1371/journal.pone.0052656
18. Quarles CC, Gochberg DF, Gore JC, Yankeelov TE. A theoretical framework to model DSC-MRI data acquired in the presence of contrast agent extravasation. *Phys Med Biol* 2009; **54**: 5749–66. doi: https://doi.org/10.1088/0031-9155/54/19/006
19. Liu HL, Wu YY, Yang WS, Chen CF, Lim KE, Hsu YY. Is Weisskoff model valid for the correction of contrast agent extravasation with combined T1 and T2* effects in dynamic susceptibility contrast MRI? *Med Phys* 2011; **38**: 802–9. doi: https://doi.org/10.1118/1.3534197
20. Bjornerud A, Sorensen AG, Mouridsen K, Emblem KE. T1- and T2*-dominant extravasation correction in DSC-MRI: part I--theoretical considerations and implications for assessment of tumor hemodynamic properties. *J Cereb Blood Flow Metab* 2011; **31**: 2041–53. doi: https://doi.org/10.1038/jcbfm.2011.52
21. Alsop DC, Detre JA, Golay X, Günther M, Hendrikse J, Hernandez-Garcia L, et al. Recommended implementation of arterial spin-labeled perfusion MRI for clinical applications: A consensus of the ISMRM perfusion study group and the European consortium for ASL in dementia. *Magn Reson Med* 2015; **73**: 102–16. doi: https://doi.org/10.1002/mrm.25197
22. Dai W, Garcia D, de Bazelaire C, Alsop DC. Continuous flow-driven inversion for arterial spin labeling using pulsed radio frequency and gradient fields. *Magn Reson Med* 2008; **60**: 1488–97. doi: https://doi.org/10.1002/mrm.21790
23. Günther M, Bock M, Schad LR. Arterial spin labeling in combination with a look-locker sampling strategy: inflow turbo-sampling EPI-FAIR (ITS-FAIR. *Magn Reson Med* 2001; **46**: 974–84. doi: https://doi.org/10.1002/mrm.1284
24. Fernández-Seara MA, Wang Z, Wang J, Rao HY, Guenther M, Feinberg DA, et al. Continuous arterial spin labeling perfusion measurements using single shot 3D GRASE at 3 T. *Magn Reson Med* 2005; **54**: 1241–7. doi: https://doi.org/10.1002/mrm.20674
25. Vidyasagar R, Abernethy L, Pizer B, Avula S, Parkes LM. Quantitative measurement of blood flow in paediatric brain tumours-a comparative study of dynamic susceptibility contrast and multi time-point arterial spin labelled MRI. *Br J Radiol* 2016; **89**: 20150624. doi: https://doi.org/10.1259/bjr.20150624
26. Ho CY, Cardinal JS, Kamer AP, Lin C, Kralik SF. Contrast leakage patterns from dynamic susceptibility contrast perfusion MRI in the grading of primary pediatric brain tumors. *AJNR Am J Neuroradiol* 2016; **37**: 544–51. doi: https://doi.org/10.3174/ajnr.A4559
27. Dallery F, Bouzerar R, Michel D, Attencourt C, Promelle V, Peltier J, et al. Perfusion

magnetic resonance imaging in pediatric brain tumors. *Neuroradiology* 2017; **59**: 1143–53. doi: https://doi.org/10.1007/s00234-017-1917-9

28. Paulson ES, Schmainda KM. Comparison of dynamic susceptibility-weighted contrast-enhanced MR methods: recommendations for measuring relative cerebral blood volume in brain tumors. *Radiology* 2008; **249**: 601–13. doi: https://doi.org/10.1148/radiol.2492071659
29. O'Connor JP, Aboagye EO, Adams JE, Aerts HJ, Barrington SF, Beer AJ, et al. Imaging biomarker roadmap for cancer studies. *Nat Rev Clin Oncol* 2017; **14**: 169–86. doi: https://doi.org/10.1038/nrclinonc.2016.162
30. Zaharchuk G, Bammer R, Straka M, Newbould RD, Rosenberg J, Olivot JM, et al. Improving dynamic susceptibility contrast MRI measurement of quantitative cerebral blood flow using corrections for partial volume and nonlinear contrast relaxivity: A xenon computed tomographic comparative study. *J Magn Reson Imaging* 2009; **30**: 743–52. doi: https://doi.org/10.1002/jmri.21908
31. Morana G, Tortora D, Staglianò S, Nozza P, Mascelli S, Severino M, et al. Pediatric astrocytic tumor grading: comparison between arterial spin labeling and dynamic susceptibility contrast MRI perfusion. *Neuroradiology* 2018; **60**: 437–46. doi: https://doi.org/10.1007/s00234-018-1992-6